Laser-induced stainless steel mesh for high effective water/oil separation

Tianchi Chen[1], *Hongtao Liu*[2] ✉, *Haifeng Yang*[1], *Wei Yan*[2], *Wei Zhu*[2], *Hao Liu*[1], *Kaijin Guo*[3]

[1]*College of Mechanical & Electrical Engineering, China University of Mining and Technology, Xuzhou 221116, People's Republic of China*
[2]*School of Materials Science and Engineering, China University of Mining and Technology, Xuzhou 221116, People's Republic of China*
[3]*Xuzhou Medical College Affiliated Hospital, Xuzhou 221116, People's Republic of China*
✉ *E-mail: Liuht100@126.com*

Published in Micro & Nano Letters; Received on 28th December 2016; Revised on 26th April 2017; Accepted on 28th July 2017

The hierarchical micro/nano structures are successfully obtained on the stainless steel mesh via a simple laser direct writing technology. The as-prepared mesh reveals excellent superhydrophilic/underwater superoleophobic properties or superhydrophobic/superoleophilic properties after 1H, 1H, 2H, 2H-perfluorodecyltriisopropoxysilane modification. According to the oil density, the superhydrophilic/underwater superoleophobic mesh allows water to permeate and repels the light oil. Its oil/water separation efficiency is as high as 98.5% for the light oil. The superhydrophobic/superoleophilic mesh can be easily wetted by heavy oils while the water will be repelled, which the separation efficiency can reach 98.0% for the heavy oil. Moreover, this special wettability mesh can still maintain high separation efficiency after 20 separation cycles, which indicates the good separation stability.

1. Introduction: In the past decades, crude oil leakage accidents and oil pollution caused by the petrochemical and food industries have become one of the most urgent global environmental problems [1]. Utilising special wettability to design oil/water separation material is a facile and effective approach to realise oil/water separation [2–4]. Recently, inspired by nature [5–7], scholars fabricated varieties of hierarchical micro/nano structures to realise special wettability surface [8, 9]. Many researchers focus on fabricate special wetting oil/water separation [10, 11]. To date, two different types of special wettability surface materials have been successfully designed, fabricated, and employed in oil/water separation in principle of oil density. Superhydrophobic and superoleophilic surface (SHBOI) can be easily wetted by oils while the water will be repelled [12]. Thus, this kind of surface is suitable for heavy oil/water separation. For the light oil/ water separation, underwater superoleophobic surface (UWSOB) allows the water to penetrate through the material easily while the oil would be repelled completely [13], for instance Zhang [14] reported underwater superoleophobic graphene oxide coated mesh with vegetable oil contact angle (CA) exceed 150°. Many methods such as dip-coating [15], vapour deposition [16], electrochemical deposition [17] and sol-gel method [18] have been employed in order to achieve above-mentioned SHBOI and UWSOB surface. However, the tedious procedures and poor mechanical durability of the surface limit their practical applications. Hence, a facile and high stability method to obtain SHBOI and UWSOB surface for oil/water separation is imperative for the practical application in oil/water separation.

Recently, many responsive oil/water separation devices have been investigated by many scholars [11]. The oil/water separation devices can change its separation model by extern field, such as pH, ultraviolet light or electric field. Feng [19] fabricated a thermo and pH dual-responsive materials for controllable oil/water separation. Water can pass through the as-prepared mesh under 55°C (pH = 7) and pH <13 (T = 25°C) while oil is kept on the mesh. When the temperature is >55°C or pH is >13, the water retention capacity of PDMAEMA hydrogel is significantly reduced. Tian *et al.* [20] reported an electric field induced water selectively permeation for oil/water separation based on the stainless steel mesh coated with root-like polyaniline nanofibers fabricated by emulsion polymerisation. Moon [21] fabricated a UV-responsive nano-sponge. This nano-sponge utilised photo-responsive $TiO_2$to realise the oil absorption and desorption.

Stainless steel mesh is a commonly used industrial filtering material, owing to its excellent anti-corrosion ability and mechanical stability. However, there is a problem still existing in realising SHBOI and UWSOB stainless steel surface. It is the adhesion problem between coating and substrate.

Herein, we fabricated SHBOI and UWSOB surface via a simple laser direct writing. The nanosecond laser direct writing is a reliable way to obtain hierarchical micro/nano structures with the comparison of femtosecond laser [9, 22], which can be easily applied to large surface area. Moreover, micro/nano structures generated by laser direct writing are original structures without consideration of the adhesion between coating and substrate. The as-prepared mesh reveals an excellent superhydrophilicity and underwater oil repellency. However, after low-energy modification, the mesh shows superhydrophobic/superoleophilic property.

2. Experiment details: Fig. 1 shows the schematic diagram of fabricating SHBOI and UWSOB stainless steel surface. Firstly, the 500# stainless steel mesh was irradiated by a focused laser beam through a laser marker with a focus lens (f = 160 mm) that can control the movement of laser beam. A commercially 25 ns laser with a working wavelength of 355 nm and repetition rate of 10.5 kHz was used as a laser source. The laser scanning routes were parallel lines. In the laser-processed step, the laser power was changed from at 366–1111.7 mW, scanning velocity was changed from 10.6 to 52.8 mm/s and laser scanning intervals was 15 µm. Following the irradiation process, the samples were cleaned with distilled water and dried at 60°C for 1 h. According to density of oil, the as-prepared sample can achieve superhydrophobicity after 2 wt% FAS-17 (1H, 1H, 2H, 2H-perfluorodecyltriisopropoxysilane) ethanol solution modification for 1 h followed by washing with ethanol and drying in an oven at 100°C for 1 h.

Surface morphologies of as-prepared surfaces were investigated by scanning electron microscope (FEI limited, Quanta 250). The sample chemical composition was studied by X-ray photoelectron spectroscopy (XPS). The water CA and sliding angle of 5 µL deionised water droplets were measured using the JC2000D-2A

doi: 10.1049/mnl.2016.0802

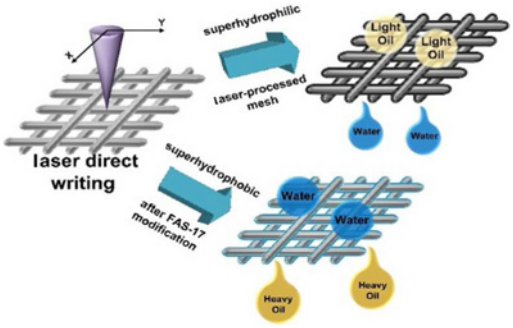

Fig. 1 *Schematic diagram of process for fabricating extremely wetting stainless steel surface*

CA measuring device on the five different points for each surface. The sample surface roughness was characterised with a Bruker's Dektak XT stylus profilers.

3. Result and discussions: Generally, laser powers and laser scanning speeds are two key factors to influence surface morphologies. Fig. 2 shows the SEM images of the different microstructures on the stainless steel meshes fabricated under different laser scanning speeds at the fixed laser powers of 831 mW. Fig. 2*a* shows scanning electronic microscopy (SEM) image of the original stainless steel mesh. The original mesh has an average pore diameter of ~40 μm, and the knitting wires have a diameter of ~40 μm. The magnified view in the inset of Fig. 2*a* reveals that the original wires have smooth surface microstructures of the untreated stainless steel mesh. After sample irradiating by focused laser beam at the lower scanning speed of 10.6 mm/s, the macroscopic morphology of the mesh did not show any significant change. However, the wire was markedly rough, as shown in Fig. 2*b*. At high magnification, as shown in Fig. 2*c*, a layer of microprotrusions decorated by hairy and globule-like aggregates composed of nanoparticles with the size from several tens to several hundred nanometres was uniformly formed on the surface of the wires. This hierarchical micro/nano structures on the mesh surface are the key factor to obtain superhydrophilicity or superhydrophobicity after FAS-17 modification. When the laser scanning speed increasing to 25.8 mm/s, as shown in Figs. 2*d* and *e*, the number of microprotrusions slightly decreases on the wire surface. The distance between microprotrusions becomes larger. Meanwhile, the hairy nanoparticles do not obviously covered on the microprotrusions. Figs. 2*f* and *g* show that the only some re-melting micro particles appear on the edge of the wire when the scanning velocity is 52.8 mm/s. Thus, the scanning speed can directly control the surface morphologies of the stainless steel mesh.

Then we fix the laser scanning speed at 25.8 mm/s and change the laser power from 366 to 1111.7 mW. Similarly there are different microstructures on the mesh wire surface as shown in Fig. 3. When the laser power is only 366 mW, there are only few random distributed microparticles on the wire surface just like structures obtained by high scanning speed as shown in Figs. 3*a* and *b*. With the increase of laser powers, more and more microparticles accumulate and cover the whole wire surface as shown in Figs. 3*c* and *d*. When the laser power increases to 1111.7 mW, some nanoparticles form by redeposition and more microparticles form on the wire surface, making the mesh surface very rough [23] (Figs. 3*g* and *h*). Thus, we can conclude that hierarchical micro/nano structures can be obtained under high laser power with relative low scanning speed. The formation of hierarchical micro/nano structures on the mesh surface at the low scanning speed is related to the single pulse energy and the number of laser pulses per irradiation spot N. N can be defined by

$$N = f/(z \times v) \tag{1}$$

where f is the laser repetition rate, z is the laser scanning line spacing, and v is the laser scanning speed. Thus, N changes from $1.3 \times 10^6/\text{cm}^2$ to $6.6 \times 10^6/\text{cm}^2$. For the lower scanning speed, N can reach as high as $6.6 \times 10^6/\text{cm}^2$, thus the surface can absorb large amount of heat per irradiation spot. Especially when the laser power is high, the heat can easily accumulates to the breaking point, the phase explosion would occur at the wire surface. Meanwhile, electrons around the irradiated region break down into dielectrics, rapidly ionise, and eventually form plasma in the high laser power [24]. The plasma will interfere the energy absorption of the ablated surface and make the splashing droplet re-deposited on the ablated region, which forms microprotrusions decorated by hairy and globule-like aggregates composed of nanoparticles. For the high scanning speed and low laser powers, it is clear that the number of laser pulses per irradiation spot decreases with scanning speed increasing. Thus the surface absorbs less heat per irradiation spot. The laser ablation only causes melting and evaporation of mesh surface. Thus, we can only find some re-melting microstructures on the wire surface.

In order to separate heavy oil, the prepared mesh surface needs to be modified by FAS-17 to achieve superhydrophobicity. Fig. 4 shows the XPS spectra of FAS-17 modified stainless steel mesh. The Si, C, F and O elements can be observed in the as-prepared

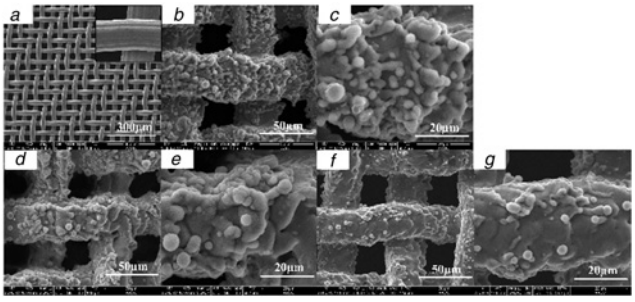

Fig. 2 *SEM images*
a Original mesh
b,c As-prepared stainless steel surface at 2000 and 5000 magnifications when the scanning speed is 10.6 mm/s
d and e As-prepared stainless steel surface at 2000 and 5000 magnifications when the scanning speed is 25.8 mm/s
f, g As-prepared stainless steel surface at 2000 and 5000 magnifications when the scanning speed is 52.8 mm/s

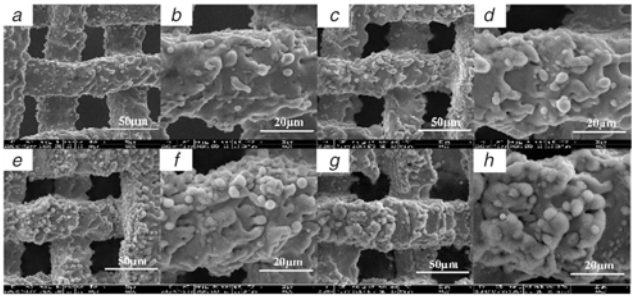

Fig. 3 *SEM images*
a, b The as-prepared stainless steel surface at 2000 and 5000 magnifications when the laser power is 366 mW
c, d The as-prepared stainless steel surface at 2000 and 5000 magnifications when the scanning speed is 568 mW
e, f The as-prepared stainless steel surface at 2000 and 5000 magnifications when the scanning speed is 831 mW
g, h the as-prepared stainless steel surface at 2000 and 5000 magnifications when the scanning speed is 1111.7 mW

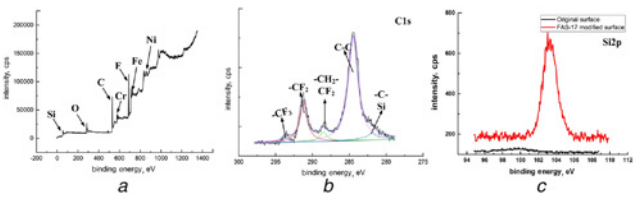

Fig. 4 *XPS spectra of the superhydrophobic surface*
a XPS survey spectra
b High-resolution of C1s
c High-resolution of Si2p

surface, as shown in Fig. 4*a*. Fig. 4*b* shows the C1s result of the XPS spectra. After decomposition and fitting, the C1s peaks locating at 293.63 and 291.22 eV are assigned to the carbon atom of $-CF_3$ and $-CF_2-$, respectively. The peaks at 288.50 and 284.49 eV are assigned to carbon atom of $-CH_2-CF_2-$ and –C–C–. The peak at 281.95 eV is attributed to the carbon atom of −C−Si. Moreover, a new peak for Si 2p was observed at 103.5 eV for the silanised sample [25], as shown in Fig. 4*c*. The XPS results indicate that FAS-17 was successfully grafted on the laser-processed mesh surface.

Fig. 5 shows the wettability of as-prepared superhydrophobic mesh surface or the underwater superoleophobic mesh surface. As shown in Fig. 5*a*, the original stainless steel mesh reveals the water CA of 103° (Fig. 5*d*), the laser-processed stainless steel mesh reveals superhydrophilicity, which the water CA is almost 0° (Fig. 5*c*). Figs. 5*g* and *h* show the gear oil CA and sliding angle of 156° and 7° when the laser-processed mesh is immersed into water. The as-prepared mesh surfaces reveal excellent underwater superoleophobicity. After FAS-17 modification, as shown in Fig. 5*b*, the laser-processed mesh shows a superhydrophobic surface with a water CA of 158° and a sliding angle of 4° (Figs. 5*i* and *j*). The water CA of the original mesh is 133° and the sliding angle is about 40° (Figs. 5*e* and *f*). The laser-processed mesh shows superhydrophobicity after FAS-17 modification. Moreover, the as-prepared superhydrophobic mesh shows superoleophilic property. The gear oil can quickly go through the superhydrophobic mesh, as shown in Fig. 5*b*.

It can be clearly seen that the laser-processed mesh reveals excellent underwater superoleophobicity. This is mainly due to the coupling interaction between massive hydrophilic hydroxyl groups (the mesh surface can absorb large amounts of ultraviolet ray and enrich the surface with hydroxyl groups [26, 27]) and the hierarchical

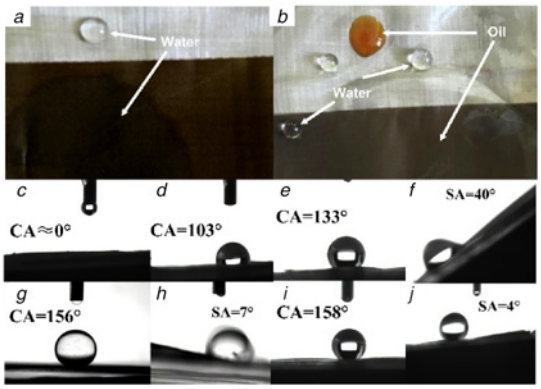

Fig. 5 *Optical image*
a Laser-processed mesh
b FAS-17 modified laser processed mesh
c,d Water CA of laser-processed mesh and original mesh
e, f Water CA and sliding angle of FAS-17 modified original mesh
g, h Gear oil CA and sliding angle of underwater laser-processed mesh
i, j Water CA and sliding angle of FAS-17 modified laser processed mesh

micro/nano structures. So when the mesh immerses into the water, the excellent superhydrophilicity help the water to stick in the hierarchical micro/nano structures, which can form a layer water to prevent the oil spreading on the mesh surface. Thus, according to underwater Cassie model, the apparent underwater oil CA θ^{co} on the laser-processed mesh could be described by (2)

$$\cos\theta^{co} = f_1(\cos\theta_1 + 1) - 1 \tag{2}$$

where f_1 is the fraction of the solid/oil interface under the oil droplet; θ_1 is the oil CA on original mesh; θ^{co} is the apparent underwater oil CA of flat stainless steel surface. In our experiment, the oil CA on original mesh is about 100°. Thus, oil droplet only contacts with 10% real contact area on the mesh surface. This can also directly prove that a large quantity of water is trapped by micro/nano hierarchical structures.

For the FAS-17 modified laser-processed mesh surface, the laser-processed mesh surface reveals excellent superhydrophobicity. Similarly to the underwater superoleophobic surface, the air can be trapped among hierarchical micro/nano structures to prevent the water wetting the mesh surface [28]. Thus, we can calculate the apparent water CA θ^{cw} according to the Cassie model as (3)

$$\cos\theta^{cw} = f_w(\cos\theta_w + 1) - 1 \tag{3}$$

where f_w is the fraction of the solid/water interface under the water droplet; θ_w is the water CA on original mesh; θ^{cw} is the apparent water CA of the flat stainless steel surface. In our experiment, the water CA of flat stainless steel surface is about 115°. Thus, water droplet only contacts with 12% real contact area on the mesh surface. This can also directly prove that the air is trapped by micro/nano hierarchical structures.

In order to further discuss the relation between different microstructures and wetting properties, we also measure the water CAs and sliding angles of samples processed with different laser scanning speeds and laser powers after FAS-17 modification. Fig. 6*a* shows a plot of water CA and sliding angles against laser scanning speed. The water CAs decrease with laser scanning speed increasing. The water sliding angles increase with laser scanning speed decreasing. Fig. 6*b* shows the roughness of samples processed by different laser scanning speed. With increasing of laser scanning, the surface roughness decreases. Thus, it can be clearly seen that after FAS-17 modification, the rougher surface leads to the bigger CA and less sliding angle, which means a superior superhydrophobicity. Similarly, the water CAs increase with laser power increasing. The water sliding angles decrease with laser scanning speed decreasing, as shown in Fig. 7*a*. The surface roughness increases with laser power increasing, as shown in Fig. 7*b*. Thus, the rougher mesh surface can greatly influence the surface wettability.

Superhydrophilic or superhydrophobic laser-processed stainless steel mesh can be used to oil/water separation according to oil density. In the light oil/water separation, as shown in Fig. 8*a*,

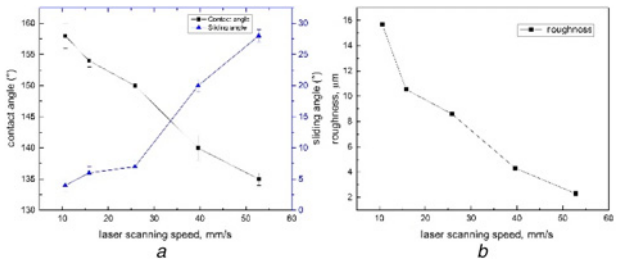

Fig. 6 *A plot of water CA and sliding angles*
a CAs, sliding angles
b surface roughness under different laser scanning speeds

doi: 10.1049/mnl.2016.0802

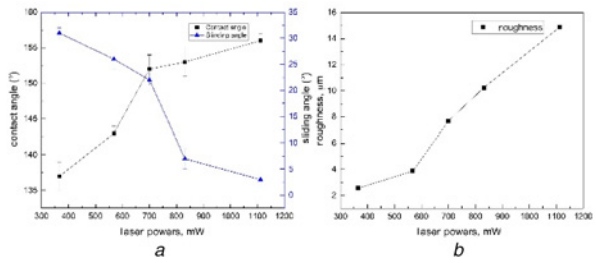

Fig. 7 *Laser scanning speed*
a CAs, sliding angles
b Surface roughness under different laser powers

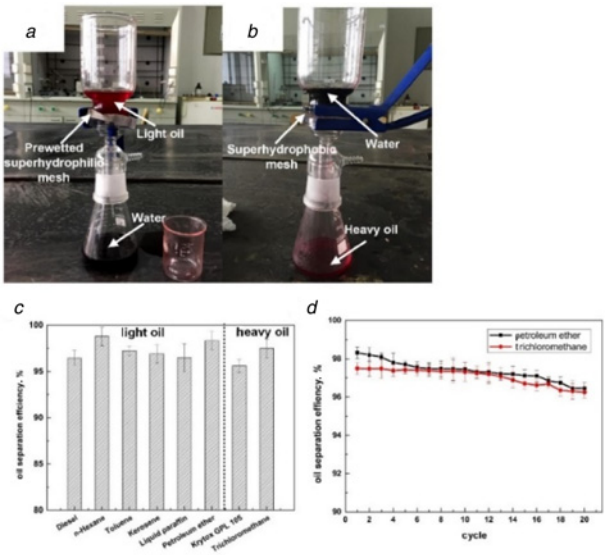

Fig. 8 *Heavy oil/water separation*
a, *b* Optical images of the oil/water separation process using the light oil and heavy oil, respectively
c Separation efficiencies for different kinds of oils
d Separation efficiencies for 20 cycles

firstly the mesh was firstly prewetted, then when a mixture solution of petroleum ether (dyed with Sudan IV) and water (dyed with the black ink) was poured onto the mesh, the black water rapidly permeated through the prewetted mesh with driving force of gravity while the petroleum ether was repelled on mesh. In the heavy oil/water separation, as shown in Fig. 8*b*. After a mixture of trichloromethane (dyed with Sudan IV) and water (dyed with the black ink) was poured on the superhydrophobic mesh, the black water was repelled on the mesh while the trichloromethane rapidly permeated through mesh. Fig. 8*c* shows the separation efficiency of light/heavy oil based on as-prepared superhydrophilic/superhydrophobic mesh. The separation efficiency was calculated according to $\eta = (m_a/m_b) \times 100$, where m_a and m_b are the mass of the water after and before the oil/water separation, respectively. Thus, according to the oil density, we can fabricate laser-processed mesh modified with different surface energy, which can separate both of light and heavy oil. The separation efficiency of the UWSOB mesh was as high as 98.5% for the hexane/water mixture, while SHBOI mesh can separate >98.0% mass of water from trichloromethane /water mixture. Moreover, after 20 separation cycles of petroleum ether/water or trichloromethane/water mixture solutions, the separation efficiency for the petroleum ether/water mixture can still reach 97.3% and the separation efficiency for the trichloromethane/water mixture are >97.2%, which indicates the good separation stability of the laser-processed meshes.

4. Conclusions: In this Letter, the superhydrophilic/underwater superoleophobic mesh or superhydrophobic/superoleophilic mesh were successfully fabricated by a simple laser direct writing and FAS-17 modification. Firstly, the mesh surface reveals superhydrophilicity after laser direct writing, which water can rapidly through the mesh. After FAS-17 modification, the laser-processed mesh shows superhydrophobicity with a water CA of 158° and sliding angle of 5° and superoleophilic property with oil CA is almost 0°. This special wettability mesh can realise the high efficient oil/water separation for both light/heavy oil and the good separation stability. It is believed that this multifunctional mesh fabricated by laser direct writing and FAS-17 modification could be a promising material for oil/water separation.

5. Acknowledgments: This work was supported by the National Nature Science Foundation of China (grant no. 51475457), Qing Lan Project, the China Postdoctoral Science Foundation Funded Project (grant no. 2015M581881), the Key Program of Science and Technique Development Foundation in Jiangsu Province (grant no. BE2015627) and a project funded by the Priority Academic Program Development of Jiangsu Higher Education Institutions.

6 References

[1] Momen G., Farzaneh M.: 'Simple process to fabricate a superhydrophobic coating', *Micro Nano Lett.*, 2011, **6**, (6), pp. 405–407
[2] Pan Y., Zhan J., Pan H., *ET AL.*: 'Microwave assisted deposition of hydroxyapatite coating on a magnesium alloy with enhanced corrosion resistance', *Mater. Lett.*, 2015, **159**, pp. 345–348
[3] Wu J., Jiang Y., Jiang D.,, *ET AL.*: 'The fabrication of pH-responsive polymeric layer with switchable surface wettability on cotton fabric for oil/water separation', *Mater. Lett.*, 2015, **160**, pp. 384–387
[4] Wan Y., Lian Z., Xu J., *ET AL.*: 'Fabrication of the stainless steel surface with super durable one-direction superhydrophobicity and two-direction anisotropic wettability', *Micro Nano Lett.*, 2014, **9**, (10), pp. 712–716
[5] Fürstner R., Barthlott W., Neinhuis C.,, *ET AL.*: 'Wetting and self-cleaning properties of artificial superhydrophobic surfaces', *Langmuir.*, 2005, **21**, pp. 956–961
[6] Kim A., Lee C., Kim H.,, *ET AL.*: 'Simple approach to superhydrophobic nanostructured Al for practical antifrosting application based on enhanced self-propelled jumping droplets', *ACS Appl. Mater. Interf.*, 2015, **7**, pp. 7206–7213
[7] Ou J., Hu W., Xue M.,, *ET AL.*: 'Superhydrophobic surfaces on light alloy substrates fabricated by a versatile process and their corrosion protection', *ACS Appl. Mater. Interf.*, 2013, **5**, pp. 3101–3107
[8] Kietzig A.-M., Hatzikiriakos S.G., Englezos P.: 'Patterned superhydrophobic metallic surfaces', *Langmuir*, 2009, **25**, pp. 4821–4827
[9] Yong J., Yang Q., Chen F., *ET AL.*: 'Stable superhydrophobic surface with hierarchical mesh-porous structure fabricated by a femtosecond laser', *Appl. Phys. A*, 2013, **111**, pp. 243–249
[10] Yu Y., Chen H., Liu Y., *ET AL.*: 'Selective separation of oil and water with mesh membranes by capillarity', *Adv. Colloid Interface Sci.*, 2016, **235**, pp. 46–55
[11] Zhang Y.L., Xia H., Kim E., *ET AL.*: 'Recent developments in superhydrophobic surfaces with unique structural and functional properties', *Soft Mat.*, 2012, **8**, (44), pp. 11217–11231
[12] Xu Z., Miyazaki K., Hori T.: 'Fabrication of polydopamine-coated superhydrophobic fabrics for oil/water separation and self-cleaning', *Appl. Surf. Sci.*, 2016, **370**, pp. 243–251
[13] Zheng X., Zhang Q., Wang J.: 'Fabrication of super-hydrophobic magnetic Fe/SiO_2 surface with tunable adhesion inspired by lotus leaf', *Micro Nano Lett.*, 2012, **7**, (6), pp. 562–563
[14] Liu Y.Q., Zhang Y.L., Fu X.Y., *ET AL.*: 'Bioinspired underwater superoleophobic membrane based on a graphene oxide coated wire mesh for efficient oil/water separation', *ACS Appl. Mater. Interf.*, 2015, **7**, (37), pp. 20930–20936
[15] Lin Y., Ehlert G.J., Bukowsky C.,, *ET AL.*: 'Superhydrophobic functionalized graphene aerogels', *ACS Appl. Mater. Interf.*, 2011, **3**, pp. 2200–2203
[16] Singh E., Chen Z., Houshmand F., *ET AL.*: 'Superhydrophobic graphene foams', *Small*, 2013, **9**, pp. 75–80

[17] Zhang B., Zhao X., Li Y.,, *ET AL.*: *RSC Adv.*, 2016, **6**, pp. 35455–35465
[18] Sun C., Zhao X.-W., Han Y.-H.,, *ET AL.*: 'Control of water droplet motion by alteration of roughness gradient on silicon wafer by laser surface treatment', *Thin Solid Films*, 2008, **516**, pp. 4059–4063
[19] Cao Y., Liu N., Fu C., *ET AL.*: 'Thermo and pH dual-responsive materials for controllable oil/water separation', *ACS Appl. Mater. Interf.*, 2014, **6**, (3), pp. 2026–2030
[20] Zheng X., Guo Z., Tian D., *ET AL.*: 'Electric field induced switchable wettability to water on the polyaniline membrane and oil/water separation', *Adv. Mater. Interf.*, 2016, **3**, (18), p. 1600461
[21] Do Hyun Kim M.C.J., Cho S.H., Kim S.H., *ET AL.*: 'UV-responsive nano-sponge for oil absorption and desorption', *Sci. Rep.*, 2015, **5**
[22] Vorobyev A., Guo C.: 'Multifunctional surfaces produced by femtosecond laser pulses', *J. Appl. Phys.*, 2015, **117**, p. 033103
[23] Jiang H.B., Zhang Y.L., Liu Y., *ET AL.*: 'Bioinspired few–layer graphene prepared by chemical vapor deposition on femtosecond laser–structured Cu foil', *Laser Photon. Rev.*, 2016, **10**, (3), pp. 441–450
[24] Bloembergen N.: 'Laser-induced electric breakdown in solids', *IEEE J. Quantum Electron.*, 1974, **10**, (3), pp. 375–386
[25] Long J., Fan P., Zhong M., *ET AL.*: 'Superhydrophobic and colorful copper surfaces fabricated by picosecond laser induced periodic nanostructures', *Appl. Surf. Sci.*, 2014, **311**, pp. 461–467
[26] Boinovich L., Gnedenkov S., Alpysbaeva D., *ET AL.*: 'Corrosion resistance of composite coatings on low-carbon steel containing hydrophobic and superhydrophobic layers in combination with oxide sublayers', *Corros. Sci.*, 2012, **55**, pp. 238–245
[27] Boinovich L.B., Emelyanenko A.M., Modestov A.D.,, *ET AL.*: 'Synergistic effect of superhydrophobicity and oxidized layers on corrosion resistance of aluminum alloy surface textured by nanosecond laser treatment', *ACS Appl. Mater. Interf.*, 2015, **7**, pp. 19500–19508
[28] Tang Y., Zhang Q., Zhan X.,, *ET AL.*: 'Superhydrophobic and anti-icing properties at overcooled temperature of a fluorinated hybrid surface prepared via a sol-gel process', *Soft Mat.*, 2015, **11**, pp. 4540–4550

doi: 10.1049/mnl.2016.0802